Vibrational Studies on Disaccharide/H_2O Systems by Inelastic Neutron Scattering, Raman, and IR Spectroscopy

C. Branca,[†] S. Magazù,*[,†] G. Maisano,[†] S. M. Bennington,[‡] and B. Fåk[‡]

Dipartimento di Fisica and INFM, Università di Messina, P.O. Box 55, Papardo, 98166 S. Agata di Messina, Italy, and ISIS Pulsed Neutron Facility, Rutheford Appleton Laboratory, Chilton, Didcot, Oxon OX110QX, United Kingdom

Received: June 7, 2002; In Final Form: November 27, 2002

Inelastic neutron scattering (INS), Raman scattering, and infrared spectroscopy experiments on pure water and on aqueous solutions of homologous disaccharides, such as trehalose and sucrose, are presented. Neutron spectra were collected by using the spectrometer MARI at the ISIS pulsed neutron source of the Rutheford Appleton Laboratory (Chilton, U.K.). The principal aim of this work is to analyze the structural modifications induced on water by trehalose and sucrose to look for different structural arrangements that can account for their different effectiveness as bioprotectors. Special emphasis was addressed to the intramolecular stretching and bending spectral contributions and to the intermolecular librational mode. A comparison of the INS spectra from pure water with those of homologous disaccharide/water mixtures showed the same peculiar behavior as found in Raman scattering, infrared spectroscopy, and computational results derived from density functional theory (DFT).

1. Introduction

Vibrational spectroscopy is one of the most widely used methods for obtaining information on materials irrespective of their state, being equally applicable to the study of gases, liquids, crystals, and amorphous solids.[1−4] Optical techniques, such as infrared and Raman spectroscopies, and inelastic neutron scattering (INS) are revealed to be ideal tools for the study of the vibrational dynamics. However, it has to be pointed out that INS spectra are different from their optical counterparts for the following reasons:

(i) Neutron wavelength and frequency transfers are 3 orders of magnitude smaller than those for photons. This means that the fluctuations observed by neutron scattering occur on correspondingly shorter spatial and time scales;

(ii) The neutron mass is of the same order as the mass of vibrating atoms and therefore the scattering process is very sensitive to the space dynamical characteristics of the system;

(iii) Neutrons interact directly with the nuclei; as a consequence, no selections rules are involved in neutron scattering.

(iv) An INS spectrum is directly proportional to the vibrational density of states weighted by the atomic mean square displacements associated with each vibrational mode and by the neutron scattering cross-sections of the constituent atoms.

A judgment of merits of different techniques is very difficult. Among the advantages of light scattering, other than the wide energy range, one can consider a good sensitivity, a high resolution, and the possibility of observing transient effects. On the other hand, as a result of the existence of spin incoherence in neutron scattering from protons, neutrons are uniquely suited for probing the single particle motions of protons in hydrogen containing substances. Moreover, the dynamic structure factor obtained from neutron scattering experiments can be directly compared to computer molecular dynamics results. This feature of INS is in contrast to the traditional optical spectroscopic techniques for which CMD calculations are possible only under some approximations.[5] For all these reasons, a fairly accurate physical picture requires the simultaneous application of many complementary techniques because such an approach allows us to probe different space-time scales and to couple with different system variables.

Starting from this consideration, we have investigated the vibrational properties of homologous disaccharide/water solutions by means of inelastic neutron scattering, Raman scattering, and infrared spectroscopy.

The structure and dynamics of hydrated disaccharides are currently the subject of an intense research effort[6−8] due to fundamental physicochemical reasons as well as to important biomedical and biotechnological applications. Among disaccharides, trehalose seems to be unique in Nature to confer many living organisms the ability to survive under extreme conditions of dehydration as well as in freezing conditions without the cumulating effects of functional stress.[9−11] In fact, notwithstanding trehalose and sucrose have the same chemical formula ($C_{12}H_{22}O_{11}$), trehalose is significantly the most effective as bioprotector.[6,7,11] Up to now, much effort has been devoted to analyze the thermoactivation and thermoprotective actions of sugars on enzymes, liposomes, and isolated biological membranes or proteins.[7,12,13] However, the molecular mechanisms underlying the bioprotective effectiveness of trehalose, whose characterization is basic for the understanding and exploitation of the potentialities of this disaccharide, have not yet been entirely understood.

In our previous and current works,[14−18] the basic hydration behavior and the structure of disaccharide solutions have been quantified as a function of concentration and temperature. In particular, Raman scattering measurements[19] showed that, among disaccharides, trehalose has the greatest destructuring effect on the tetrahedral hydrogen bonded network of water,

* Corresponding author. E-mail: magazu@dsme01.unime.it.
[†] Università di Messina.
[‡] Rutheford Appleton Laboratory.

10.1021/jp026255b CCC: $25.00
Published on Web 01/14/2003

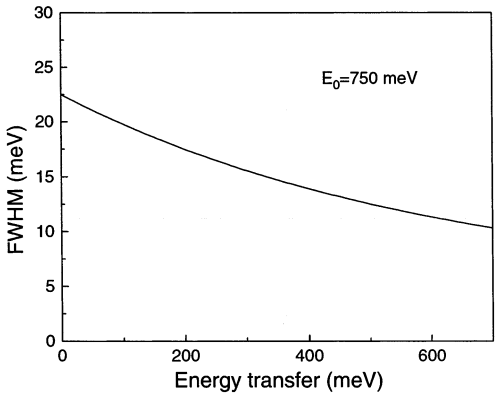

Figure 1. Energy resolution (fwhm) as a function of energy transfer.

the same that on lowering temperature gives rise to ice. As a result the amount of freezable water is reduced and the crystallization process is obstructed. More recently, several studies by quasi elastic neutron scattering (QENS) experiments[20] suggested that trehalose affects significantly the dynamics of water molecules in its neighborhood consistently with the presence of a series of hydration layers or shells, each of which is characterized by a relatively slow diffusion. Finally, the different rigidity of both trehalose/H_2O and sucrose/H_2O mixtures has been characterized by means of neutron scattering measurements,[21] providing information on the low-frequency dynamics and on the thermal mean square atomic fluctuations through the temperature behavior of the Debye−Waller factor.

The fundamental information that finally emerges from previous studies is that the bioprotective effectiveness of disaccharides reflects a complex array of interactions that derive from the unique properties of the water molecules. Despite considerable research efforts,[22−25] it is extremely difficult to explain in a coherent fashion the complexity of the water nature, essentially because of the poor understanding of the H-bond interaction. Solute-induced perturbations in water structure are, in turn, less well understood than the structure of pure water. For example, contrary to the case of water, inelastic neutron scattering investigations for disaccharide/water solutions are still lacking, despite neutron scattering appearing to be particularly suitable to get direct information about the H-bond interaction.

In the present work we analyze, through a joint employment of INS, Raman scattering, and infrared spectroscopy, the structural modifications induced by the presence of trehalose and sucrose on the hydrogen bond network of water to evidence different structural arrangements that can account for their different effectiveness as bioprotectors. Special emphasis will be addressed to the intramolecular stretching and bending spectral contributions and to the intermolecular librational mode.

2. Experiment

A pure sample of dihydrated α,α-trehalose and sucrose were purchased from Aldrich-Chemie. Measurements were performed on disaccharide aqueous solutions at different molar fractions ϕ, $\phi = n_d/n_d + n_w$, n_d and n_w being the solute and water mole numbers, respectively.

INS Measurements. Inelastic neutron scattering measurements were carried out on the MARI direct geometry time-of-flight spectrometer at the ISIS pulsed neutron facility of the Rutheford Appleton Laboratory (Chilton, U.K.). The incident energy was 750 meV and the energy resolution (full width at half-maximum, fwhm) varied from 22 meV for elastic scattering to 10 meV at an energy transfer of 700 meV, as illustrated in Figure 1. The detectors covered scattering angles from 3−135°. The sample container consisted of two concentric thin-walled aluminum cylinders of inner and outer diameters of 5.0 and 4.9 cm, respectively. The annular space between the cylinders was filled with the sample. Measurements were performed at $T = 293$ K on pure water and on sucrose/H_2O and trehalose/H_2O solutions at different molar fractions. An empty container run was made to correct the scattering from the sample holder.

Data were corrected for background and container scattering and transformed to the dynamical structure factor as a function of wave vector and energy, $S(Q,\omega)$, using standard data-reduction routines at ISIS. Monte Carlo calculations of the multiple scattering were made using the MSCAT code. The measured spectra were used as input for the calculation, which was iterated until convergence. Within the energy and wave-vector range of interest, it was found that the multiple scattering is structureless with a smooth increase in intensity with increasing energy transfer. No correction for multiple scattering was therefore done.

As with all H_2O-hydrated hydrocarbons, the ratio of protons to other nuclei is larger than 1. Therefore the spectra measured are essentially due to incoherent scattering from the protons. The calculated total bound scattering cross-section of $C_{12}H_{22}O_{11}\cdot 19H_2O$, corresponding to a molar fraction $\phi = 0.05$, is 5.11 kbarn (1 kbarn $= 10^{-21}$ cm^2); 0.30 kb of this value is due to coherent scattering so that the contribution of the latter to the total cross-section amounts to nearly 5.9%. For the $C_{12}H_{22}O_{11}\cdot 10H_2O$ samples, corresponding to $\phi = 0.09$, the total bound scattering cross-section is 3.6 kbarn with a coherent scattering contribution to the total cross-section of nearly 6.4%. Therefore, the time-of-flight spectrum of the neutrons scattered from our samples is essentially the incoherent double differential cross-section of hydrogen atoms.

Raman Scattering Measurements. Raman scattering measurements were performed at $T = 293$ K on pure water, trehalose, and sucrose aqueous solutions at different molar fraction values. Before measurements the samples were stored in the dark and left for a long time for equilibration; they have been filtered with an Amicon filter of 0.45 μm diameter pores to obtain dust-free solutions. Then the samples were sealed in optical quartz cells of inner diameter 5 mm and mounted in an optical thermostat especially built to avoid any unwanted stray-light contributions. The measurements were performed with a temperature stability better than 0.1 °C. The samples of high purity, as well as the optical purity of the sample holder, ensured collecting data with a good signal-to-noise ratio and with high reproducibility. I_{VV} and I_{VH} Raman spectra were obtained by a high resolution fully computerized Spex-Ramalog 5 triple monochromator in a 90° scattering geometry. Vertically polarized radiation of an INNOVA 70 Series Ar−Kr gas mixed laser operating in the 4579−6764 Å was used as an excitation source. To reduce fluorescence we chose the 6471 Å laser line. The laser power was mantained at approximately 1 W. The detection apparatus consisted of a photon counting system whose outputs were processed on line by a computer. The scattered photons were automatically normalized for the incoming beam intensity to ensure good data reproducibility. To separate the scattering due to the solution from the background, which was almost entirely due to either the Raman scattering or fluorescence of the quartz cell, it was assumed in the removal procedure that the intensity in some distinct spectral regions was due entirely to quartz and other types of noise. This is only approximately correct because a detectable sample intensity at all frequency values exists. However, in comparison with the OH stretching features, the intensity of these spurious contributions is negli-

gible and the assumption is useful. The uncertainty in this correction forms the principal uncertainty in the spectra and was estimated to be less than ±2% of peak intensity for an I_{VH} spectrum and less than ±0.5% of peak intensity for an I_{VV} spectrum.

Each reported spectrum is the average of different scans. For each isotherm spectrum, the individual I_{VV} and I_{VH} scans were taken in an alternating sequence to ensure that a definite intensity relationship existed between the final I_{VV} and I_{VH} spectra of the some isotherm. Isotropic scattering intensities were calculated from the parallel and perpendicular components of the scattered light by $I_{iso} = I_{VV} - {}^4/_3 I_{VH}$. Different spectral regions have been measured with a different energy resolutions ranging between 4 and 2 cm^{-1}. All disaccharide/H_2O spectra were normalized with the C−H stretching band that does not suffer H-bond interactions.

IR Measurements. Fourier transform infrared spectra were taken by a Bomem DA8 Fourier transform infrared (FTIR) spectrometer working with a globar lamp source, a KBr beam splitter, and DTGS/KBr detector. In this configuration it has been possible to cover the 400−4000 cm^{-1} range with a resolution of 4 cm^{-1}. To avoid saturation effects due to the high transmission of water, measurements on pure water and on disaccharide/H_2O solutions have been performed by attenuated total reflection infrared (ATR-IR) spectroscopy.

To obtain a good signal-to-noise ratio, 32 repetitive scans were automatically added for each measurement. For all the samples the experimental data were deconvoluted into the minimum number of symmetrical Voigt profiles $V(\omega)$. This distribution, the most suitable for band shape analysis, is a convolution of a Gaussian and a Lorentzian curve

$$V(\omega) = \frac{\int_{-\infty}^{+\infty} \frac{a_0 \exp(-y^2)\,dy}{a_3^2 + \left[\left(\frac{\omega - a_1}{a_2}\right) - y\right]^2}}{\int_{-\infty}^{+\infty} \frac{\exp(-y^2)\,dy}{a_3^2 + y^2}}$$

where a_0 and a_1 are the amplitude and the center of the distribution, respectively, a_2 is a width related to the Gaussian half width at half-maximum, and a_3 is a width depending on the ratio of the Lorentzian half-width at half-maximum to a_2.

3. Results and Discussion

As it is well-known, vibrational spectroscopy typically explores peak locations to identify compounds, probes rotations and bond length, or provides information about the interactions between molecules through shifts in band frequencies and line widths from their gas-phase values.[26,27] Following the essential aspects of line shape theory, we first analyze the water spectra obtained by INS, Raman scattering, and infrared spectroscopy; see Figure 2. The INS spectrum has been obtained by summing the spectra over Q values ranging between 1 and 10 $Å^{-1}$. This Q range was chosen to minimize the large Debye−Waller factor, which lowers the intensity of the curves summed over the higher angle detectors as energy transfer increases. To improve the shot-noise ratio, the isotropic Raman spectrum has been obtained by summing the spectra obtained on three limited frequency ranges with a different integration time and resolution. Finally, the ATR-IR spectrum covers the 100−500 meV energy range.

A free water molecule has just three normal modes of vibration: two of them, ν_1 and ν_3 (ν_1 = 453.4 meV and ν_3 = 465.7 meV), depend on the force constant for stretching the covalent O−H bond, whereas the bending mode ν_2 (ν_2 = 197.7 meV) depends on the force constant for changing the bond angle. In liquid water the spectra are more complex due to several types of vibrational interactions.[28] The vibrational spectrum of liquid water can be conveniently discussed in terms of two regions: an *intramolecular* region, occurring for ω > 124 meV, and an *intermolecular* region at lower frequencies.

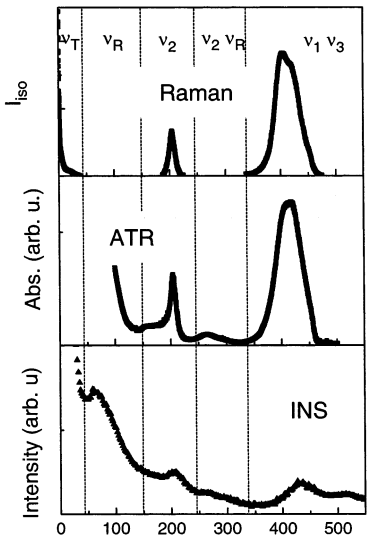

Figure 2. INS, Raman, and ATR-IR spectra of water at T = 293 K. The INS spectrum is at $\langle Q \rangle$ = 7.45 $Å^{-1}$.

The *intermolecular* region includes the weak bands below 35 meV corresponding to the restricted translational motions of H_2O molecules involved in direct hydrogen bond interactions. This region is labeled ν_T. The restricted rotational region, within 37 and 124 meV, labeled ν_R, reflects the librational motions of H_2O molecules arosen from restraints produced by hydrogen bonds.

Concerning the *intramolecular* region, it encompasses the bending mode ν_2 centered around 204 meV in Raman and infrared spectra, or 207 meV in INS spectra, and a broad band between 347 and 471 meV identified with the OH stretching mode, that is, with the normal modes ν_1 and ν_3. The small hump at 280 meV, is assigned to a combination of OH librational, ν_R, and bending modes, ν_2. Finally, a combination band clearly appears in the high-energy region of the INS spectrum around 508 meV. It has been assigned to the overtone of the librational and stretch bands on the basis of frequency shifts analysis.[29] As can be seen from Figure 2, the spectral contributions obtained by different techniques show different spectral features because the three techniques do not measure equivalent quantities.

Let's now analyze in more detail the OH stretching mode. It is a fact[30] that the O−H stretching in water, due to the presence of the hydrogen bond, shows a red shift and a large broadening with respect to the gas phase. Its spectral shape can be related to the distribution of H-bonds and is determined by the distribution of the forces acting on the internal degrees of freedom, causing a shift and an inhomogeneous broadening due to the anharmonicity of the oscillators.

The presence of the isoskedastic point in the isotropic spectrum of pure water suggested to some authors[2] the decomposition of each spectrum into two classes of OH oscillators with an opposite temperature dependence, the so-called "open" and "closed" contributions. The first one has been attributed to O−H vibrations in tetrabonded H_2O molecules that have an "intact bond" and originate low-density patches in the

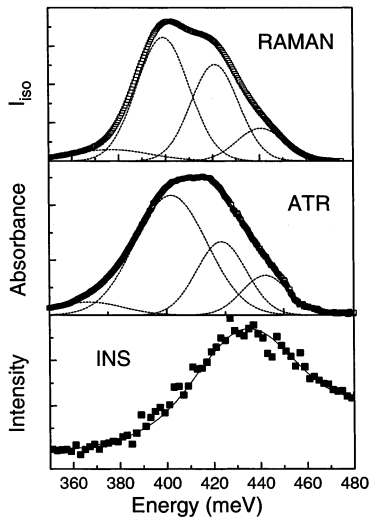

Figure 3. Raman, ATR-IR, and INS OH stretching mode of pure water with the respective Gaussian components at $T = 293$ K.

TABLE 1: Numerical Curve Fit Parameters Relative to the ATR-IR and Raman OH Stretching Mode of Pure Water

pk ctr (meV)	fwhm	% area
	ATR-IR	
367	39.0	6
402	36.1	58
423	25.1	24
442	23.3	12
	Raman	
376	34.6	6
399	26.2	50
421	23.6	32
440	24.1	12

system. The second class of oscillators corresponds to O−H vibrations of H_2O molecules that have a partially developed hydrogen bond (distorted bond). The open Gaussian component is centered near 398 meV, whereas the closed one is centered near 424 meV.[1] It is noteworthy that with declining temperature, one finds that the "open" contribution increases, indicating an enhanced hydrogen bonding that gives rise to patches of four bonded water molecules.

In Figure 3 the Raman, ATR-IR, and INS OH stretching bands of pure water at $T = 293$ K are reported. The experimental spectra have been fitted by Gaussian functions (also shown in the figure). As expected, the spectral line shapes show differences related to the different properties of vibrations. In particular, four Gaussian components were required to fit both the Raman and infrared spectra, whereas only one single Gaussian fits very well the single broad INS OH stretching mode. The infrared and Raman parameters obtained from the fitting procedure are listed in Table 1. As can be seen, the peak frequencies agree very well with each other.

As can be seen from Figure 3, in the Raman spectrum an inflection point is visible around 410 meV, whereas it is absent in the infrared spectrum. The absence of the inflection point can be justified by considering that the half-widths of the low-frequency infrared components are larger than the corresponding Raman values. The obtained fitting parameters (see Table 1) are in good agreement with previous experimental studies.[28] Finally, concerning the INS spectrum, the OH stretching mode is centered at a higher frequency and its contour has a significantly different shape with respect to the Raman and infrared spectrum. In fact, the different vibrational properties involved in a neutron scattering experiment, together with the effect of multiple scattering, make more visible the inhomogeneous broadening of the OH stretching mode in the INS spectrum in comparison with the infrared and Raman spectra. However, the choice of a single Gaussian as fitting function is in agreement with previous inelastic neutron studies.[31] According to these studies, the stretching vibrational band shifts to higher energies as the temperature is increased; at the same time, the combination band was revealed to be strongly temperature dependent, becoming sharper and increasing in center energy as the temperature is lowered to that of the supercooled state. Ricci and Chen[31] and Ricci et al.[32] have proposed a specific mechanism that allowed them to correctly predict both the frequency shift and the intensity of the satellite peak as a function of temperature. According to this perturbative analysis the energy shift of the combination band is directly proportional to the mean value of the hydrogen-bond strength, which decreases as the temperature rises above room temperature. Contrary, the OH stretch softening, observed in going down to the supercooled state, has been rather attributed to the formation of more intact hydrogen bonds between neighboring molecules at lower temperatures, which tends to soften the intramolecular attractive bond. Moreover, above room temperature, a strong increase of the combination band peak intensity, I_2, has been observed, whereas a decrease has been observed for the stretch band, I_1. Because the intensities I_1 and I_2 are related to the number of intact bonds, P, and broken bonds, $(1 - P)$, respectively,[25] the strong increase of I_2 above room temperature reflects an increased number of broken bonds as the temperature rises, so confirming previous conclusions.

TABLE 2: Peak Frequencies of the Stretching, ω_3, and Combination Bands, ω_4, of Pure Water, Together with the Values of the Parameter $P/(1 - P)$ and of the Hydrogen Bond Mean Strength Parameter, D, for Pure Water at Different Temperatures

T (K)	ω_3	ω_4	I_1/I_2	$P/(1-P)$	D_2 (kcal/mol)
258[a]	428	514	3.54	3.31	3.16
293[b]	432	508	1.69	1.68	2.91
313[a]	435	494	1.11	1.21	2.41
353[a]	437	496	0.71	0.63	2.46

[a] Reference 25. [b] Present work.

Starting from the considerations reported above, we have evaluated from the fitting parameters both the hydrogen bond mean strength parameter, D, and the ratio $P/(1 - P)$ at $T = 293$ K. The obtained values are reported in Table 2 together with the values from literature data[25] at different temperatures. The D value calculated from our data agrees very well with those reported in the literature.[25] Moreover, starting from the evaluation $P = 1.8 - 0.004T$ (ref 33), the calculations show that the ratio I_1/I_2, also reported in Table 2, agrees with the ratio $P/(1 - P)$ to better than 1% against 10% of previous determinations.[25]

Taking into account these observations, before considering the disaccharide/water mixtures, we have first analyzed the main spectral features of trehalose dihydrate and sucrose starting from the computational results[34] derived from DFT for the gas phase and the monohydrate crystal of trehalose. The computation has provided a detailed picture for the interpretation of the vibrational properties of the trehalose/H_2O system, although the description of the intermolecular interactions and of the harmonic dynamics can be only moderately accurate. By DFT, vibrational eigenvalues and eigenvectors have been obtained by diagonalization of the dynamical matrix. Moreover, the infrared activity of each mode has been evaluated (see Figure 4) by using an approximate expression. From the simulation of the monohydrate crystal structure, the following points emerge:

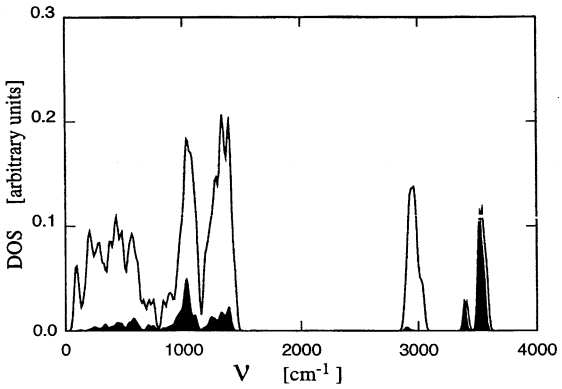

Figure 4. Vibrational spectrum of the gas-phase trehalose molecule. The infrared activity is given by the black area under the lower curve (Ballone, P.; et al. *J. Phys. Chem. B* **2000**, *104*, 6313).

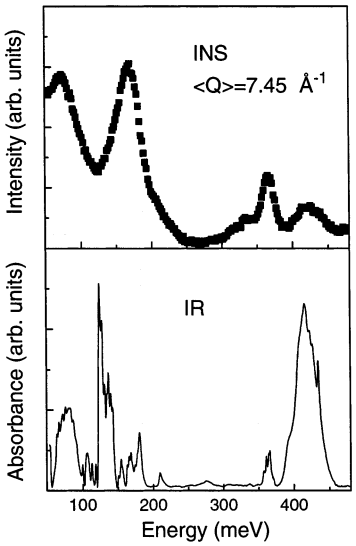

Figure 5. INS and IR spectrum of trehalose dihydrate at $T = 293$ K.

•The OH stretching of water gives rise to two isolated peaks at 389 and 421 meV.

•The pure OH stretching of trehalose gives rise to a band from 391 to 404 meV broader than in the gas-phase molecule.

•The CH stretching modes give rise to a band extending from 354 to 377 meV, which is contaminated by some OH stretching characters. These modes are separated by a large gap from the band of the hybridized H−C−H, C−C−H, and C−O−H bending modes, observed between 145 and 177 meV. The stretching of the C−O bonds occurs in a range between 120 and 136 meV, whereas it is difficult to assign a well-defined character to the modes below 117 meV, however, the oscillations of the OH groups around the minimum of the C−C−O−H torsional potential have been localized at energies between 55 and 70 meV, with the exception of the OH group giving rise to the intramolecular hydrogen bond, whose torsional mode has an energy of 86 meV.

The computational results are consistent with the experimental infrared and neutron data; see Figure 5. In particular, the highest frequency bands ($\omega > 86$ meV) appear at nearly the same frequency as in the computation and therefore they can be identified with confidence. In more detail, in the FT-IR spectrum of trehalose dihydrated one can recognize the O−H stretching mode (≈415 meV) and the double peaked C−H stretching mode (360 and 365 meV). In the OH stretching region a strong sharp band at 434 meV is clearly visible, attributed to the stretching modes of the OH groups considered to be more or less free.

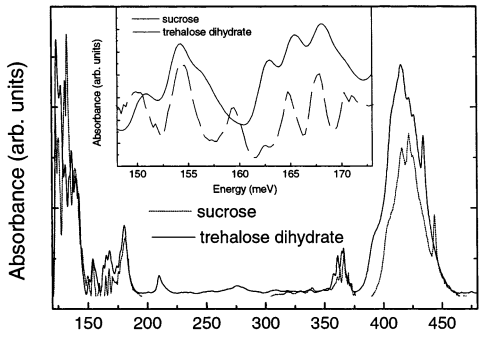

Figure 6. Comparison between the IR spectrum of trehalose dihydrate and sucrose. In the inset a magnification of the OH deformations region is reported.

The presence of the two H_2O molecules in the trehalose dihydrate sample, besides broadening the OH stretching mode, gives rise to a broad band around 272 meV, assigned to a combination of OH librational and bending modes, as well as to a band peaked around 209 meV attributed to the H−O−H bending of water. At intermediate energies (124−186 meV) we find the contributions coming from the stretching of C−C and C−O groups and from the C−H bending. In particular, the spectral contributions at 162, 165, and 169 meV have been assigned to OH deformations, whereas the broad band observed at 181 meV has been tentatively assigned to CH_2 scissoring vibration. At lower energies ($\hbar\omega < 124$ meV) the peaks, corresponding to skeletal and collective vibrations, are not very well resolved. However, the peaks observed at 123 and 118 meV have been attributed to the antisymmetric and symmetric stretching modes of the glycosidic bond.[35]

For what concerns the INS spectrum of trehalose dihydrate, the most pronounced spectral contributions are those related to the vibrations that imply large amplitude oscillations of the hydrogen atoms, that is, the OH stretching mode, around 420 meV, the CH stretching mode, around 365 meV, with an extended low-frequency wing, a slight shoulder at 209 meV, due to the HOH bending mode, a single broad peak around 170 meV, encompassing all the OH deformations, and the CH_2 scissoring mode, and finally the librational band at 72 meV.

By comparison of the infrared spectrum of trehalose and sucrose (see Figure 6), the most apparent difference concerns the total absence in the sucrose spectrum of all the crystal water contributions present in the trehalose dihydrate spectrum, indicating that no water is detectable in the sample. An upshift of the sharp peak ($\omega \approx 444$ meV) in the OH stretching region is also observable; moreover, substantial differences in the OH distortion bands are present; see the inset of Figure 6. We will see that the analysis of these latter bands is of particular importance to obtain information on the crystallinity degree of the disaccharide/water solutions.

Let us turn now the attention on the disaccharide/H_2O solutions spectra. These spectra have been first normalized with the C−H stretching band, which does not suffer H-bond interactions. As an example, in Figures 7 and 8 the infrared and INS spectra of trehalose dihydrated and of trehalose/water solutions at $\phi = 0.09$ and $\phi = 0.05$ are reported. As is evident from first sight, some common features are detectable in both the IR and INS spectra. First, the intensity of the hydration water contributions increases as the disaccharide concentration diminishes. In particular, with reference to the OH stretching mode, we can observe a slight downshift of the peak frequency and a broadening of this mode as the water content increases, indicating the presence of a wider variety of hydrogen bonds.

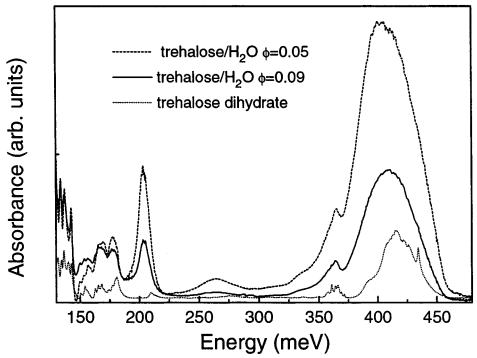

Figure 7. IR spectra of trehalose dihydrate and trehalose/H_2O mixtures at $\phi = 0.09$ and $\phi = 0.05$.

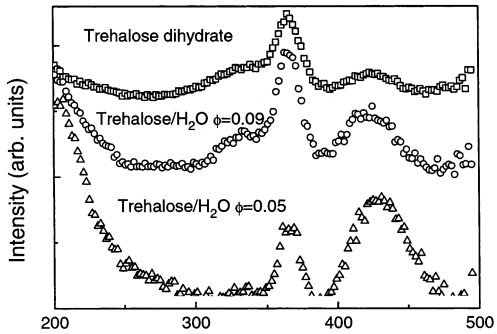

Figure 8. INS spectra of trehalose dihydrate and trehalose/H_2O solutions at different concentrations.

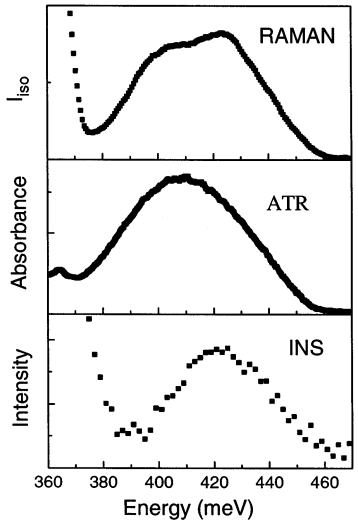

Figure 9. Raman, ATR-IR, and INS OH stretching modes of trehalose/H_2O mixture at $\phi = 0.09$ and at $T = 293$ K.

Contrary to the OH stretching mode, the CH stretching modes are relatively unchanged in frequency peaking but become broader as the disaccharide concentration diminishes. Second, we can observe a downshift in the peak position of the HOH bending mode and a broadening of the OH deformations peaks, particularly visible in the infrared spectra. With reference to these latter spectra, it is also interesting to note that the peak at 434 meV disappears, probably because when the water concentration increases, all the OH groups are bonded.

In the following we focus on the spectra of trehalose and sucrose/H_2O mixtures at $\phi = 0.09$ obtained by different techniques. In Figures 9 and 10 we have compared the INS, Raman, and ATR-IR intramolecular OH stretching modes of trehalose and sucrose/H_2O mixtures at $\phi = 0.09$, respectively. As can be seen, the most interesting information on the structural

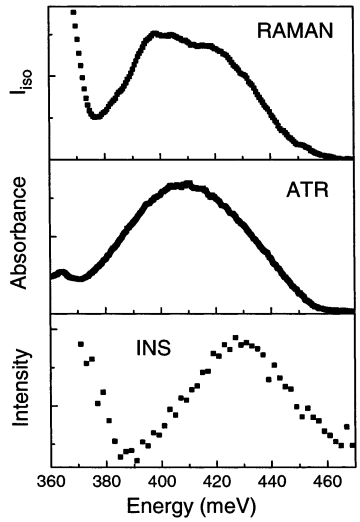

Figure 10. Raman, ATR-IR, and INS OH stretching modes of sucrose/H_2O mixture at $\phi = 0.09$ and at $T = 293$ K.

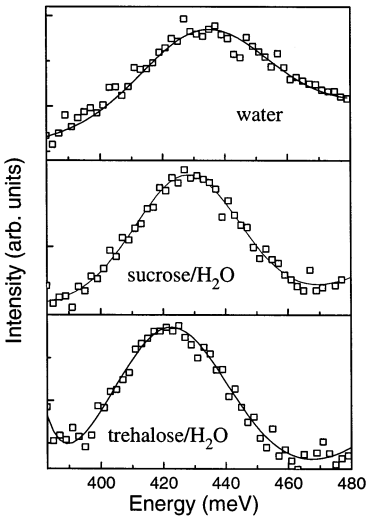

Figure 11. INS spectra of water, trehalose/H_2O, and sucrose/H_2O mixtures, $\phi = 0.09$, at T = 293 K and $\langle Q \rangle = 0.745$ Å^{-1}.

properties of disaccharide water mixtures can be drawn from the Raman and INS spectra with respect to the ATR-IR spectra. By comparing the Raman OH stretching band from pure water with that of trehalose and sucrose/H_2O mixtures at $\phi = 0.09$, one finds that, among homologous disaccharides, trehalose promotes the most substantial changes on the hydrogen bond network. In fact, by decomposition of each isotropic Raman spectrum into an "open" and a "closed" contribution, it has been observed that, at a same concentration, trehalose promotes a more marked decrease of the fractional "open" band intensity. Because this contribution, as discussed above, is related to the presence of a tetrahedric H-bonded network in pure water, we can therefore argue that trehalose promotes the most extensive layer of structured water around its neighborhood.

We will see now that this observation is confirmed by INS evidences. As a preliminary step, we have summed the INS spectra over Q values ranging between 1 and 10 Å^{-1} and normalized the disaccharide solutions spectra with the C−H stretching band. In Figure 11 a comparison of the INS OH intramolecular stretching band of water, trehalose/H_2O, and sucrose/H_2O mixture at $\phi = 0.09$ is reported; the fitting Gaussian functions are also shown in the figure. When the spectra are compared, a more marked downshift of the OH stretching mode and a greater narrowing of the bandwith for the trehalose/H_2O

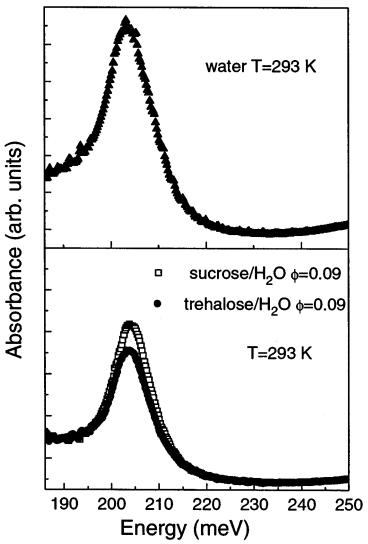

Figure 12. Comparison of the ATR-IR bending modes of pure water and of trehalose and sucrose/H_2O mixtures at $\phi = 0.09$.

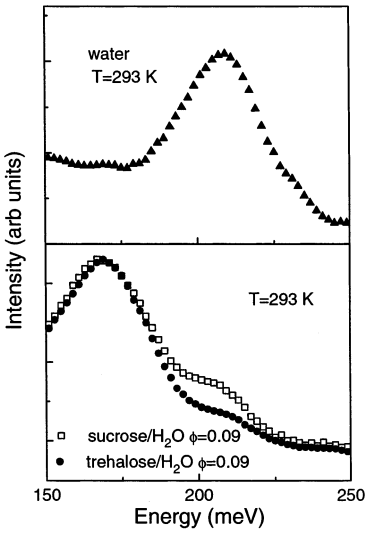

Figure 13. Comparison of the INS bending modes of water and of trehalose and sucrose/H_2O solutions at $\phi = 0.09$ and $\langle Q \rangle = 0.745$ Å^{-1}.

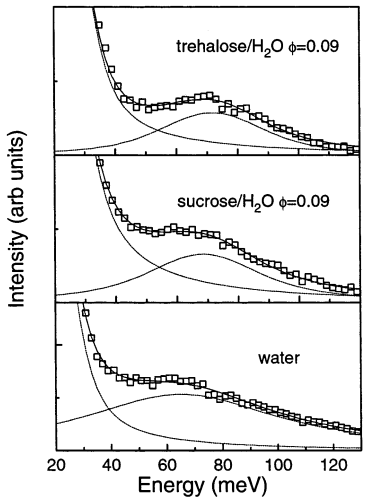

Figure 14. Comparison of the intermolecular librational band of water, trehalose/H_2O, and sucrose/H_2O mixture at $\phi = 0.09$ at $T = 293$ K. The Gaussian components and the resulting fitting functions are also shown.

mixture than for the sucrose/H_2O mixture is observed. It is more than reliable to hypothesize that, at this intramolecular level, the interactions played in the two disaccharide water mixtures are of the same nature. As a consequence, the effect of the intramolecular forces on the intramolecular vibrations will be the same. On the contrary, what is substantially different in the two mixtures is the number of bonds between each disaccharide molecule and the neighboring water molecules. Therefore, the lower frequency peak position of the trehalose/H_2O mixture can be justified by the highest value of its hydration number in comparison with that of the sucrose/H_2O mixture, as has been inferred also from density and ultrasonic velocity measurements[15−17] and MD simulations.[36] The existence of a different structural arrangement is also testified by the different bandwidth of the OH stretching mode in the two disaccharide/H_2O mixtures. In particular, the narrower band observed in the trehalose/H_2O mixture is indicative of the presence of a more ordered structure, which implies longer time correlation processes.

The analysis of the intramolecular HOH bending mode supports this hypothesis. As is well-known, by observing this mode, we can obtain more direct information on the structural modifications induced on water by disaccharides, because in the bending region there is no overlap between the water and sugar peaks. As emerges from the IR and INS spectra (see Figures 12 and 13), respectively, also in this case the presence of trehalose tends to modify more markedly the bending mode of pure water, which results in less intensity for the trehalose/H_2O mixture in comparison with the sucrose/H_2O mixture. Moreover, by analyzing the trehalose/H_2O spectra at different concentrations, we observe that increasing the water content decreased the center frequency of the bending mode, tending to a plateau value corresponding to the characteristic center frequency of pure water (204 meV). This behavior has been only evidenced in the trehalose/H_2O solutions. In fact, in the sucrose/H_2O solutions spectra the peak position of the bending mode is centered around 204 meV and does not change by increasing the water concentration. Finally, it is worthwhile that although infrared data indicate that the plateau value is reached at $\phi \approx 0.09$, according to the INS spectra this plateau is reached at a higher water concentration. In fact, as we can observe from Figure 13, the bending mode of trehalose/H_2O solution at $\phi = 0.09$ is still upshifted with respect to the bending mode of water.

Evidence of a relevant modification in the hydrogen bond network of pure water also emerged by analyzing the INS intermolecular librational band; see Figure 14. To study the low-energy spectral regions, we summed the spectra over Q values ranging between 1 and 3 Å^{-1}. The respective Gaussian components and the resulting fitting functions are also shown in the figure. As reported above, the librational band of water occurs at 60 meV and arises from the electrostatic Coloumbic interaction between neighboring molecules. The analysis of these spectra has evidenced the presence of a more marked upshift in the position of the librational band of the trehalose/H_2O mixture compared to that of the sucrose/H_2O mixture at the same concentration. In fact, the fitting parameters show that this band is shifted to 65 meV for the sucrose/H_2O mixture and to 72 meV for the trehalose/H_2O mixture.

Due to the intermolecular nature of the vibrational properties observed, this upshift can be explained by hypothesizing a stronger hydrogen bond interaction in the trehalose/water mixture than in the sucrose/water mixture. This hypothesis is supported by previous density and ultrasonic velocity measurements that have evidenced that, with respect to other disaccharides, the trehalose/water system is characterized, in a wide

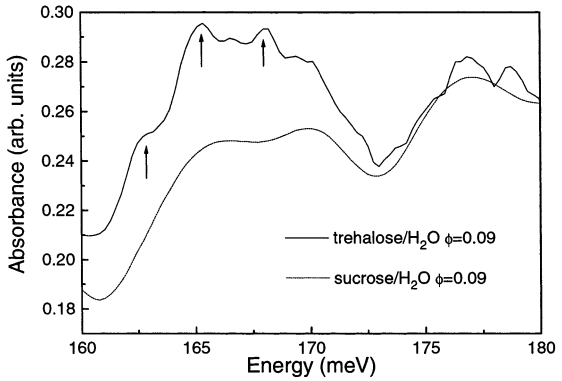

Figure 15. Comparison of the ATR-IR spectra of trehalose and sucrose/H_2O mixtures at $\phi = 0.09$. The arrows indicate the OH deformation peaks.

concentration range, by the highest value of the solute−solvent interaction strength.[15,17] This result has been successively confirmed by QENS measurements,[21] which have allowed us to recognize the trehalose/H_2O mixture as the "strongest" system compared to the sucrose/H_2O mixture at the same concentration. Moreover, comparison of the spectral features of the two disaccharide/H_2O mixtures suggests the presence in the trehalose/H_2O mixture of highly symmetric in-phase oscillations, indicative of a greater degree of crystallinity of this system at high concentration. This hypothesis is also confirmed by the presence of well resolved OH deformation peaks in the infrared spectrum of the trehalose/H_2O mixture at $\phi = 0.09$, which are not particularly evident in the sucrose/H_2O spectrum at the same concentration; see Figure 15.

Conclusions

In the present work we analyzed the structural modifications induced by the presence of homologous disaccharides on the main spectral features of pure water.

The comparison of different spectral contributions of pure water with those of trehalose and sucrose/H_2O mixtures indicates that the presence of homologous disaccharides tends to modify differently the configurational arrangements of pure water.

The changes observed in the intramolecular modes have been justified by the different hydration numbers of the trehalose and sucrose/H_2O mixtures. A different interpretation has been proposed to explain the differences emerged in the intermolecular librational band. In fact, in this case the more marked upshift of the librational peak position of the trehalose/H_2O mixture has been explained by hypothesizing a stronger hydrogen-bond interaction in the trehalose/water mixture than in the sucrose/water one. This hypothesis is supported by previous QENS measurements, which allowed us to recognize the trehalose/H_2O mixture as the "strongest" system compared to the sucrose/H_2O mixture.

All these findings evidence the presence in the trehalose/H_2O mixture of a more ordered nanoscale structure that, although able to adapt the trehalose/water complex to the irregular surface of the biostructures, encapsulates them into more "rigid" structures. This, in our opinion, can account for the greater bioprotective effectiveness of trehalose.

References and Notes

(1) Walrafen, G. E. *Water: A Comprehensive Treatise*; Plenum: New York, 1971.

(2) D'Arrigo, G.; Maisano, G.; Mallamace, F.; Migliardo, P.; Wanderlingh, F. *J. Chem. Phys.* **1981**, *75*, 4264.

(3) Bansil, R.; Wiafe-Akenten, J.; Taaffe, J. L. *J. Chem. Phys.* **1982**, *76*, 2221.

(4) Yeh, Y.; Bilgram, J. H.; Kanzig, W. *J. Chem. Phys.* **1982**, *77*, 2317.

(5) Bansil, R.; Berger, T.; Toukan, K.; Ricci, M. A.; Chen, S. H. *Chem. Phys. Lett.* **1986**, *132*, 165.

(6) Nwaka, S.; Holzer, H. *Progress in Nucleic Acid Research and Molecular Biology*; Academic Press: New York, 1997; p 197.

(7) Crowe, J. H.; Carpenter, J. F.; Crowe, L. M. *Annu. Rev. Physiol.* **1998**, *60*, 73.

(8) Crowe, J. H.; Crowe, L. M.; Chapman, D. *Arch. Biochem. Biophys.* **1985**, *236*, 289.

(9) Vegis, A. *Annu. Rev. Plant Physiol.* **1964**, *15*, 185.

(10) Clegg, J. S. *Comp. Biochem. Physiol.* **1967**, *20*, 8.

(11) Green, J. L.; Angell, C. A. *J. Phys. Chem.* **1989**, *93*, 2880.

(12) Sun, W. Q.; Leopold, L. M.; Crowe, L. M.; Crowe, J. H. *Biophys. J.* **1996**, *70*, 1769.

(13) Hottiger, T.; De Virgilio, C.; Hall, M. N.; Boller, T.; Wiemken, A. *Eur. J. Biochem.* **1994**, *219*, 187.

(14) Magazù, S.; Maisano, G.; Migliardo, P.; Middendorf, H. D.; Villari, V. *J. Chem. Phys.* **1999**, *109*, 1170.

(15) Branca, C.; Magazù, S.; Maisano, G.; Migliardo, F.; Migliardo, P.; Romeo, G. *J. Phys. Chem. B* **2001**, *105*, 10140.

(16) Magazù, S.; Migliardo, P.; Musolino, A. M.; Sciortino, M. T. *J. Phys. Chem. B* **1997**, *101*, 2348.

(17) Branca, C.; Magazù, S.; Maisano, G.; Migliardo, P. *J. Biol. Phys.* **2000**, *26*, 295.

(18) Magazù, S.; Maisano, G.; Migliardo, P.; Tettamanti, E.; Villari, V. *Mol. Phys.* **1999**, *96*, 381.

(19) Branca, C.; Magazù, S.; Maisano, G.; Migliardo, P. *J. Chem. Phys.* **1999**, *111*, 281.

(20) Magazu, S.; Villari, V.; Migliardo, P.; Maisano, G.; Telling, M. T. F. *J. Phys. Chem. B* **2001**, *105*, 1851.

(21) Branca, C.; Magazù, S.; Maisano, G.; Migliardo, F. *Phys. Rev. B* **2001**, *64*, 224204.

(22) Brockhouse, B. N. *Phys. Rev. Lett.* **1959**, *2*, 287.

(23) Harling, O. K. *J. Chem. Phys.* **1969**, *50*, 5279.

(24) Chen, S. H.; Toukan, K.; Loong, C. K.; Price, D. L.; Teixeira, J. *Phys. Rev. Lett.* **1984**, *53*, 1360.

(25) Toukan, K.; Ricci, M. A.; Chen, S. H.; Loong, C. K.; Price, D. L.; Teixeira, J. *Phys. Rev. A* **1988**, *37*, 2580. The inelastic incoherent neutron scattering studies of water began in 1958 when Brockhouse using a reactor source, observed the low-energy part of the inelastic scattering spectra of this liquid. In 1969 Harling measured its high-energy component due to internal vibrations. However, due to the low flux of neutrons in the reactor source he used, the measured stretch vibrational band occurred at a wave-vector transfer Q that is far too large for this excitation to have any appreciable intensity. It was not until spallation neutron sources came into existence that neutron scattering from high-energy excitations in liquid water became practical. In fact, the availability of intense neutron beams from pulsed spallation sources opened the possibility of observing a chemical bond breaking in the neutron scattering processes particularly in the case of an incoherent neutron scattering from a bound proton or a hydrogen atom because of its unusually large scattering cross-section.

(26) Schweizer, K.; Chandler, D. *J. Chem. Phys.* **1982**, *76*, 2296.

(27) Knapp, E. W.; Fisher, S. F. *J. Chem. Phys.* **1982**, *76*, 4730.

(28) Walrafen, G. E. *J. Chem. Phys.* **1967**, *47*, 114. Walrafen, G. E. *J. Chem. Phys.* **1964**, *40*, 3249.

(29) Walrafen, G. E.; Blatz, L. A. *J. Chem. Phys.* **1973**, *59*, 2646.

(30) Magazù, S.; Maisano, G.; Majolino, D.; Migliardo, P. *Proc. Int. Conf. Properties Water Steam; Phys. Chem. Aqueous Syst.: Mtg. Needs Ind., 12th* 317, 1995.

(31) Ricci, M. A.; Chen, S. H. *Phys. Rev. A* **1986**, *34*, 1714.

(32) Ricci, M. A.; Chen, S. H.; Price, D. L.; Loong, C. K.; Toukan, K.; Teixeira, J. *Physica B* **1986**, *136*, 190.

(33) Stanley, H. E.; Teixeira, J. *J. Chem. Phys.* **1980**, *73*, 3404.

(34) Ballone, P.; Marchi, M.; Branca, C.; Magazù, S. *J. Phys. Chem. B* **2000**, *104*, 6313.

(35) Wolkers, W. F.; Oldenhof, H; Alberda, M.; Hoekstra, F. A. *Biochim. Biophys. Acta* **1998**, *83*, 1379.

(36) Conrad, P. B.; de Pablo, J. J. *J. Phys. Chem. A* **1999**, *103*, 4049.